Turbulence, Heat and Mass Transfer 10

Unsteady heat transfer analysis of an impinging jet with high-order spectral element methods

C. De Michele[1], A. Aiello[1] and G. Coppola[1]
[1]*Dipartimento di Ingegneria Industriale, Università degli Studi di Napoli 'Federico II', Piazzale Tecchio, 80, 80125 Napoli, Italy carlo.demichele2@unina.it, alessand.aiello@studenti.unina.it, gcoppola@unina.it*

Abstract – Numerical simulations are a powerful tool to understand the kinematic and thermodynamic behaviour of impinging jet, which is of great interest in many industrial application. However, in addition to the usual difficulties of computer simulation of incompressible fluid motion and heat exchange, this flow also presents the added issue of involving severely truncated open boundaries. The most commonly used boundary conditions either cause numerical instabilities or have an exceedingly high computational cost.

A two-dimensional simulation of the confined impinging jet at $Re = 2500$ with a non-dimensional nozzle-to-plate distance $H/D = 2$ has been used to test the effectiveness of alternative boundary conditions designed to correctly reproduce the physics of the phenomenon. A large eddy simulation of the three-dimensional case with the same parameters has been performed as well. In both cases, the boundary conditions prevented the divergence of the simulation and the production of non-physical reflections.

1. Introduction

Impinging jets are a topic of great interest because of their importance and widespread usage in industrial applications, especially if heat transfer is considered. They are useful in all those situations in which cooling, heating, drying, or mixing is required and, in general, where there is a need for high-transport properties. Relevant examples are provided by cooling jets for electronic devices or for turbines and rocket engine casings, but also for propellant injections in liquid or hybrid motors.

Despite the extensive amount of work done in studying and characterizing these devices, some of their physical aspects are not fully understood yet, due to the complexity of the flow field [1]. For instance, the influence of the vortical structures on the heat exchange and on the presence of a second peak of Nusselt number is still an active research topic. Moreover, in many technological applications, research is still needed to find the optimal configuration to maximize the efficiency of the cooling (number of nozzles, inlet's shape, angle of impingement, synthetic perturbation, roughness of the impingement wall, curvatures, and so on) and the heat-transfer rate, for both heating and cooling purposes, is typically a function of a large number of parameters, such as Reynolds and Prandtl numbers, and of geometric features like the nozzle-to-plate distance.

Besides classical experimental investigations, impinging jets are also studied numerically, especially in the case of a single impinging jet on a flat, smooth surface. For most real cases, impinging jets work at relatively large Reynolds numbers, which can be complicated to reproduce in computational fluid dynamics (CFD) simulations, due to both the complexity of the required numerical setting to prevent instabilities and the resulting computational cost. In addition to that, one of the main challenges in this type of configurations is the setting of boundary conditions, as its type and the mathematical formulation can greatly influence the overall results. The inlet velocity profile (if velocity is chosen to define the inlet) is important to characterize the stagnation region and the first vortical structures, whereas the thermal boundary conditions on both the impingement plate and the confinement walls must be chosen in such a way that the

physical problem to simulate is well represented; a Neumann-type boundary condition on the impingement plate and Dirichlet-type boundary conditions on the confinement walls are interesting choices for many industrial applications. No-slip condition is prescribed on every solid boundary.

The most challenging aspect of the boundary conditions belongs to the outlets. Especially when confinement walls are present and the nozzle-to-plate distance is not so large, the flow on the outlets presents irregular and hardly predictable structures (this is particularly true for three-dimensional simulations), and many strategies have been developed and tested through the years. Unless a very wide domain is built, which is often unfeasible due to high computational cost, a channel-type velocity profile does not suit the realistic behavior of the fluid, as it may create strong instabilities due to the sudden forcing exerted on it to match that condition. If the aim of the study is to analyze the flow field relatively near the stagnation region, the *fringe region technique* [2] allows to progressively bring the fluid to the chosen outflow condition, avoiding instabilities with an accurate selection of the modulating parameters, but still non-realistic trends are observable and, usually, what happens near the outlets should not be taken in exam. This leads to the necessity of performing calculations on computational grids which are more extended than needed and ignoring what happens close to outflows, with an important increase in computational cost. An interesting breakthrough has come recently with the formulation of energy-stable *open boundary conditions* (OBC) [3, 4], derived directly from the assumption that, on the boundaries, numerical energy must not increase or decrease.

In the present work, the incompressible Navier-Stokes equations are solved through high-order spectral-element methods in Nek5000 in order to simulate the flow field around the jet and the heat exchange at the wall. Numerical simulations of two- and three- dimensional confined impinging jets have been performed at $Re = 2500$ and $Pr = 1$, with a nozzle-to-plate distance of two jet diameters. The novel feature of the present analysis is an assessment of the conditions imposed on the open boundaries, which is a known source of numerical instabilities [5] as well as possible numerical artifacts [4]. Open boundary conditions have been implemented in the solver through user-defined subroutines and the results allowed to shorten the computational domain and to reduce the overall computational cost.

2. Nek5000 solver

Nek5000 is a high-order open-source scalable CFD solver, for the solution of incompressible and low Mach number Navier-Stokes equations and heat transfer problems. It is a highly scalable code and, for this reason, it can be efficiently used on the parallel architecture of high-performance computing machines. The code is based on the Spectral Element Method (SEM) and provides a wide range of polynomial orders, typically order $N = 5 \div 15$ in space, but in general it is possible to choose until $N = 32$. However, the suggested value for optimal performance is around 7. For time integration, backward differentiation formulas with order accuracy from one to three.

Multiple kinds of boundary conditions are available in Nek5000 for both fluid velocity and temperature or other passive scalars. For the velocity, aside from periodic and Dirichlet boundary conditions, also Neumann conditions can be chosen. In this case, the value of pressure on the boundary is imposed, which can be used to model an outflow boundary condition. For this condition, the so-called "Do-nothing" open boundary condition, the equation that is solved on the boundary is

$$-p\,\hat{\mathbf{e}}_\mathrm{n} + \frac{1}{Re}(\boldsymbol{\nabla V}) \cdot \hat{\mathbf{e}}_\mathrm{n} = 0 \tag{1}$$

in which p is the pressure, $\boldsymbol{V}$ is the velocity vector, Re is the Reynolds number and $\hat{\mathbf{e}}_\mathrm{n}$ is the unit vector normal to the boundary.

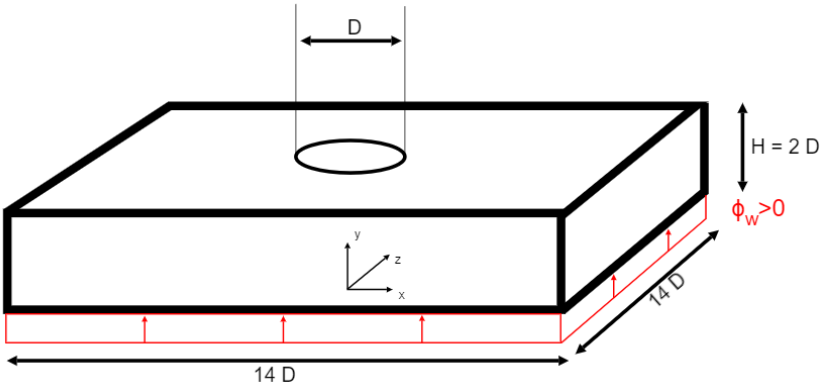

Figure 1: Schematic of the domain of the confined round jet impinging on a heated wall.

An additional possible treatment of the open boundary is offered by the tools included in the KTH Framework developed by the KTH Royal Institute of Technology, which extend NEK5000 capabilities by including the fringe region technique [2]. The idea of this method is to include, in a region adjacent to the open boundary, a forcing term $\boldsymbol{F}$ which gradually brings the velocity to its desired value $\widetilde{\boldsymbol{V}}$, which is the target velocity, to make a smoother transition to the Dirichlet condition. The formula for the forcing term is

$$\boldsymbol{F} = \lambda(x)\left(\boldsymbol{V} - \widetilde{\boldsymbol{V}}\right) \tag{2}$$

in which the one-dimensional fringe function $\lambda(x)$ controls the strength of the forcing term.

For the passive scalar, here exemplified by temperature T, it is possible to impose periodic, Dirichlet, Neumann or Robin boundary conditions. The Neumann one allows the choice of heat flow on the boundary as

$$\kappa(\boldsymbol{\nabla} T)\cdot\hat{\mathbf{e}}_{\mathrm{n}} = \phi \tag{3}$$

in which κ is the thermal conductivity and ϕ the heat flux. This can be used to model both a wall with a fixed heat flux or an open boundary.

3. Numerical setup

The object of the simulations is a confined cooling jet impinging on a heated wall. Two walls are present: one at the bottom on which the jet is impinging, and one on to top from which the jet originates. The distance H between those walls is an important parameters that has a strong influence on the jet behaviour [6]; a value $H/D = 2$, in which D is the jet diameter, has been chosen. For both walls, no-slip boundary conditions are considered; on the bottom wall, a constant heat flux $\varphi = 0.04$ has been imposed; for both the top wall and the jet the temperature is fixed at $T_j = 0.1$.

The jet inlet profile is another condition that can greatly affect the flow field and heat exchange. The velocity profile chosen for the vertical velocity v is

$$v = -\frac{n+2}{n}\left(1 - \left(\frac{2r}{D}\right)^n\right) U_b \tag{4}$$

with bulk velocity $U_b = 1$ and $n = 28$, which is the one used by Dairay et al. [7] to approximate the results of the experimental data reported in [5]. The variable r is the radial distance from the axis of the jet, which in the two-dimensional case reduces to $|x|$.

A more complex issue is the choice of the conditions to impose on the open boundaries, due to the truncation of the unbounded domain, to prevent instabilities and avoid spurious effects inside the domain. The use of the standard open boundary condition in Eq. (1) caused the simulation to diverge once the vortices had reached the edge of the domain. The fringe region method has been used before, e.g., in [7], to allow the vortices to exit the domain without causing instabilities. This, however, implies the use of a non-physical forcing in a region of the domain that must be sufficiently far away from the region of interest in order not to affect the results of the simulation. This technique results in the use of a domain that is generally much greater than the one that could be otherwise used, with a consequent increase in the computational cost of the simulation.

The way that has been chosen in the present work is the boundary condition identified as "OBC-C" in [3], which is defined by the equation

$$-p\hat{\mathbf{e}}_\mathrm{n}+\frac{1}{Re}(\boldsymbol{\nabla V})\cdot\hat{\mathbf{e}}_\mathrm{n}-\left[(\theta+\alpha_2)\frac{1}{2}\|\boldsymbol{V}\|^2\hat{\mathbf{e}}_\mathrm{n}+(1-\theta+\alpha_1)\frac{1}{2}(\boldsymbol{V}\cdot\hat{\mathbf{e}}_\mathrm{n})\boldsymbol{V}\right]\Theta_0(\hat{\mathbf{e}}_\mathrm{n},\boldsymbol{V})=0 \tag{5}$$

in which the parameters must satisfy the inequalities $0\leq\theta\leq 1$ $\alpha_1\geq 0$ $\alpha_2\geq 0$. For our simulations we chose $\theta=1$, $\alpha_1=1$, $\alpha_2=0$. In the equation also appears the smoothed step function $\Theta_0(\hat{\mathbf{e}}_\mathrm{n},\boldsymbol{V})$, defined as

$$\Theta_0(\hat{\mathbf{e}}_\mathrm{n},\boldsymbol{V})=\frac{1}{2}\left(1-\tanh\frac{\boldsymbol{V}\cdot\hat{\mathbf{e}}_\mathrm{n}}{\delta U_b}\right) \tag{6}$$

in which δ controls the sharpness and has been set to 0.05.

A similar difficulty is presented by the choice of the correct conditions on the open boundary for temperature. The use of the Neumann condition in Eq. (3) with zero heat flux causes non-physical reflections inside the domain that affect the thermodynamic evolution. On the other hand, better results have been found by applying the energy-stable condition presented in [4] which, omitting the unsteady term, is given by

$$\kappa(\boldsymbol{\nabla}T)\cdot\hat{\mathbf{e}}_\mathrm{n}=[(\boldsymbol{V}\cdot\hat{\mathbf{e}}_\mathrm{n})T]\,\Theta_0(\hat{\mathbf{e}}_\mathrm{n},\boldsymbol{V}) \tag{7}$$

This condition solved the reflection problem and did not cause the alteration of the field upstream, but only had a local impact on the temperature field of the vortices exiting the domain. Using this conditions it has been possible to limit the size of the domain, with a width $14D$.

For the three-dimensional case, a subgrid-scale model has been employed to avoid the resolution of the smallest scales in the regions sufficiently far away from the wall and reduce the computational cost. Nek5000 model is based on a high-pass filter and described in [8].

The Reynolds number of the simulations is based on the bulk velocity U_b and $Re=2500$. The Prandtl number Pr has been chosen equal to 1, so for the Peclet number we have $Pe=Re$.

4. Results

Two-dimensional impinging jets represent an important step to understanding the main features of the flow field and to test numerical setup. They are a very useful test-case to study the behavior of the implemented boundary conditions under critical conditions, since the fluid cannot develop along a radial direction as it would happen for three-dimensional cases and, as a result, vortical structures and backflows are stronger on the open boundaries.

Results obtained with 2D simulations allowed us to validate the numerical performances of the code and to understand the critical issues in terms of stability. For instance, the implemented schemes allowed to solve the flow field with a relatively coarse mesh and the explicit/implicit schemes together with the Operator-Integrator Factor Scheme (OIFS) [9] made it possible to

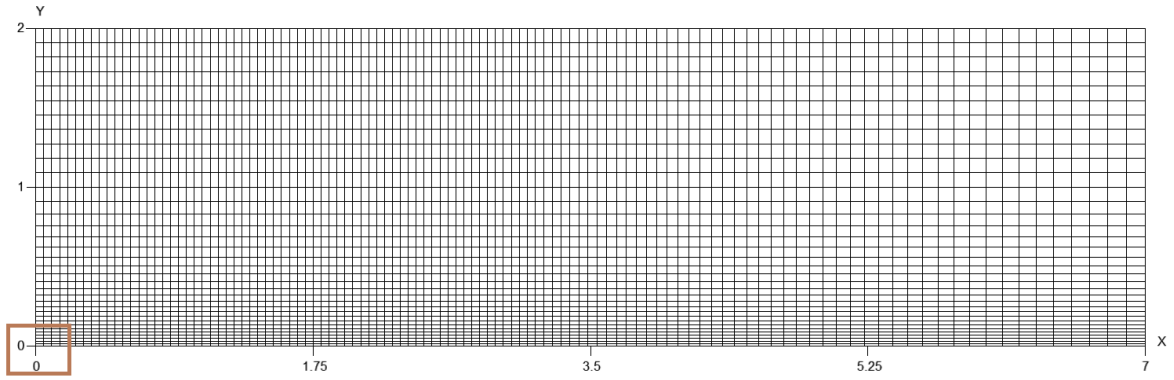

(a) *Mesh showing the rectangular elements.*

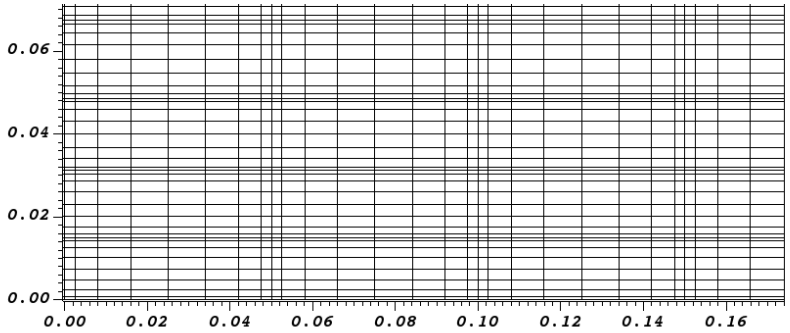

(b) *GLL points.*

Figure 2: Two-dimensional mesh and GLL points.

work at high Courant numbers ($c = 2.5$ in the current simulation). The whole simulation has been carried out to a final time $t_f = 250$.

4.1 Meshing strategy and flow field description

The initial computational grid has been obtained by means of the software Gmsh. For the current simulation, a mesh of 7700 quadrilateral elements has been built and, once the Gauss-Lobatto-Legendre (GLL) points are collocated, the result is the one shown in Fig. 2 (where only the right half is represented due to symmetry). A polynomial order $N = 8$ has been selected to achieve the target accuracy and to work inside the optimized range of Nek5000. The computational grid is uniform in x-direction for $-2.75 \leq x \leq 2.75$ to capture both the jet axis' structures and the vortices formation close to it, while a non-uniform mesh has been used for $2.5 \leq |x| \leq 7$, becoming coarser towards the boundaries. Regarding y- direction, more accuracy is provided in correspondence of the impingement wall to capture the main structures as well as the main quantities of interest such as the mean and instantaneous Nusselt number.

A first representation of the velocity vector field at $t \simeq 37$ is reported in Fig. 3a which depicts the instantaneous velocity field. After an initial transient, the flow field exhibits a roll-up region near the jet axis which is caused by counter-rotating vortices near the upper wall that are, in turn, generated by the primary vortices (direct evolution of the vortices on the jet axis) observed for $x \approx \pm 2$. The vortices' formation and shedding appear to be correlated to the second peak in mean Nusselt number [10], which will be analyzed in Sec. 4.2. In fact, Fig. 3(b) (reporting the velocity field averaged in time) shows that the primary vortices give higher velocities near the impingement plates in the region $2 \leq |x| \leq 3$. Convective phenomena are prevalent in this region which is also the zone where we observe an increase in mean Nusselt number through

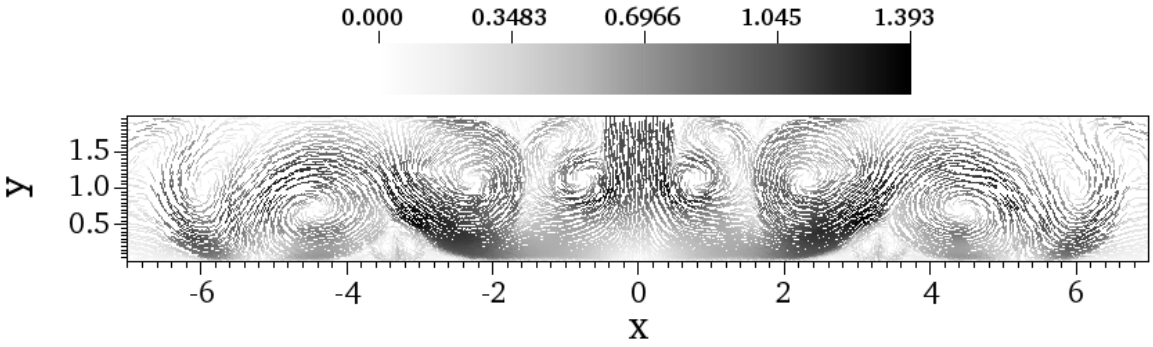

(a) *Instantaneous velocity field ($t = 36.7$)*

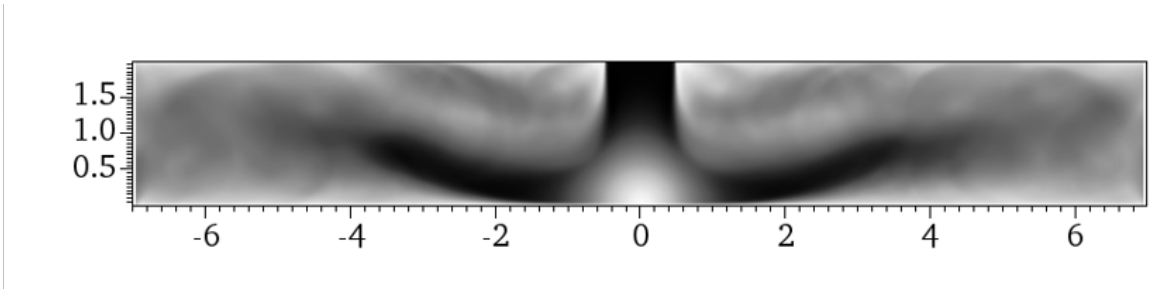

(b) *Averaged velocity field.*

Figure 3: Instantaneous and averaged velocity field.

its second peak. Secondary vortices can also be seen at $x \approx \pm 3.2$ and they are of particular relevance because they represent the reattachment of the boundary layer and its thickening. Lastly, we notice that the flow field is still fairly symmetrical (although small asymmetries can be already seen between left and right sides) so it is still possible to refer to half of the domain only. For $t \geq 50$ there are visible changes in heat transfers between the two sides and, for $t \geq 60$ the asymmetry becomes visible also on the velocity field.

4.2 Heat transfer analysis

In this Section we focus on the heat-transfer analysis by inspecting the temperature fields and the Nusselt number, which is defined as:

$$Nu(\boldsymbol{x},t) = \frac{\phi_w D}{\kappa(T(\boldsymbol{x},t) - T_j)}. \tag{8}$$

In Eq. (8) ϕ_w is the flux density at the wall (fixed by the Neumann boundary condition) and T_j is the temperature of the jet at the inlet, which is fixed by the Dirichlet boundary condition and specified in such a way that the jet has a cooling action on the plate. As shown in [7], for the given H/D we expect a second peak in mean (i.e. averaged in time) Nusselt number $\langle Nu \rangle$. This local maximum is shown in Fig. 4, where both sides of the domain have been shown for an averaging time-span $\Delta t_{\text{avg}} = t_{\text{fin}} - t_{\text{in}} = 40$, where the initial time has been taken as $t_{\text{in}} = 20$ to remove the initial transient. The local secondary maximum is located at $x \approx \pm 2.5$ which, by inspecting Fig. 3, is highly correlated with the separation point of the boundary layer. Due to the occurrence of the primary vortices, the flow separates and forms a bubble-like zone where recirculation transports heat away from the wall. Because of this phenomenon, wall temperature decreases and the Nusselt number reaches a peak before decreasing again where the fluid reattaches.

To fully understand the physics behind the observed results it is useful to also consider

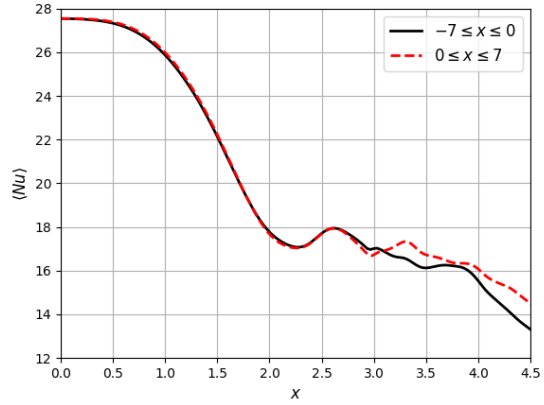

Figure 4: Secondary peak of the mean Nusselt number.

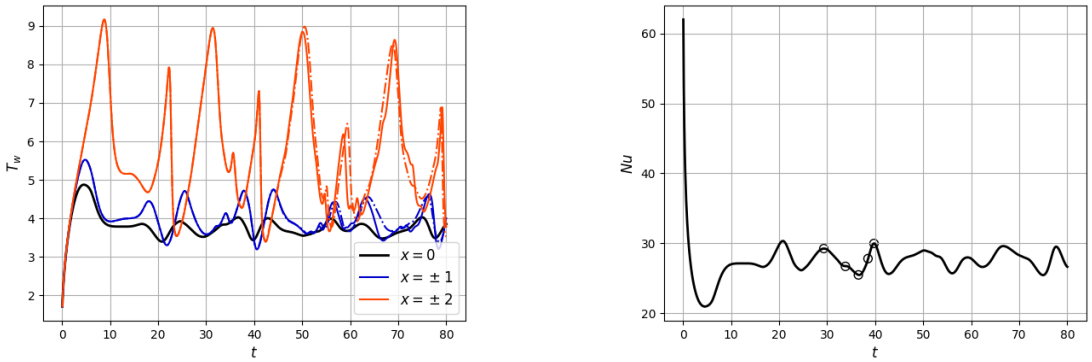

(a) Wall-temperature evolution at different x. Dashed lines refer to negative values of x.

(b) Instantaneous stagnation Nusselt number. The five points highlighted are used in Fig. 6.

Figure 5: Temperature and Nusselt number time evolution for the two-dimensional impinging jet.

the instantaneous velocity and temperature fields, and the instantaneous spatial distribution of the Nusselt number. The cyclic formation of the primary and secondary vortices is expected to influence also the instantaneous temperature field, as well as the variation in time of the Nusselt number at fixed stations. Note that, because of definition (8) and the Neumann boundary conditions on the impingement wall, as well as the assigned value of T_j at the inlet, the relation $Nu \sim T_w^{-1}$ can be obtained. Thus, we first report wall-temperature (T_w) evolution in time for fixed stations along x.

Fig. 5a reports the wall temperature as a function of time at several fixed stations. The plot shows the cooling action of the jet, which starts impinging on the heated wall at $t \approx 5$, and induces an oscillating evolution of the wall temperature around a mean value, different for each x. For $x = \pm 2$ this happens with some delay due to the time required by the fluid to reach those stations, and we can also see that the further we move away from the stagnation point, the larger the oscillations around the mean value become. The corresponding temporal evolution of the stagnation Nusselt number $Nu_{\text{stag}}(t) = Nu(\mathbf{0}, t)$ is reported in Fig 5b. Before the jet impinges on the heated wall, the temperature increases due to the positive flux ϕ_w and so Nu_{stag} decreases, then, it stabilizes around a mean value. Inside the interval $29.3 \leq t \leq 39.7$, which can be roughly identified as a "cycle" in the evolution of the wall temperature, five time

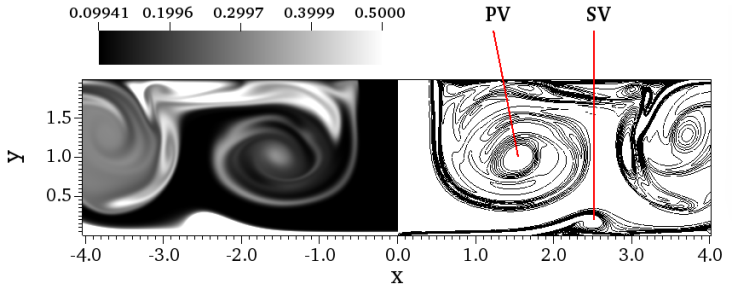

(a) $t = 29.3$

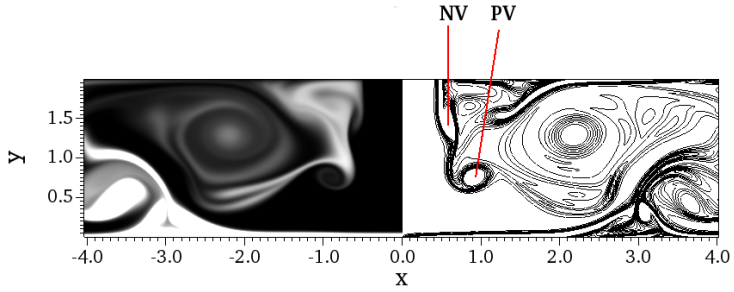

(b) $t = 33.6$

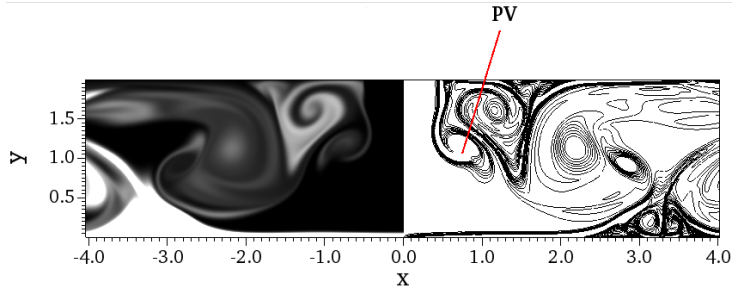

(c) $t = 36.4$

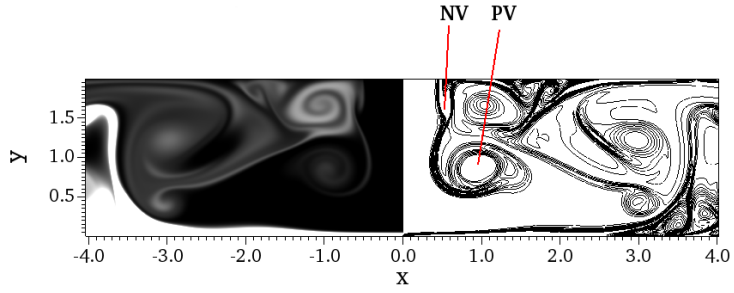

(d) $t = 38.6$

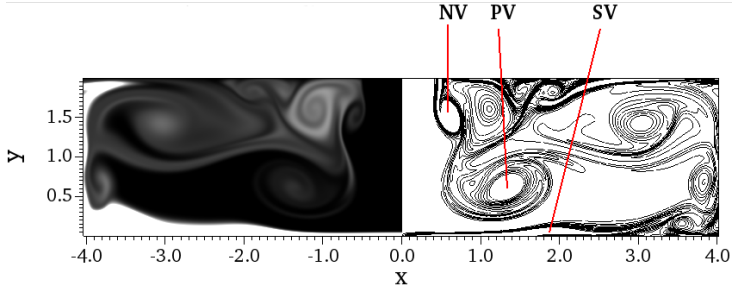

(e) $t = 39.8$

Figure 6: Temperature field (left) and vorticity (right) in correspondence of the five points highlighted in Fig. 5b. Superior limit for temperature is set at 0.5 for visualization purposes.

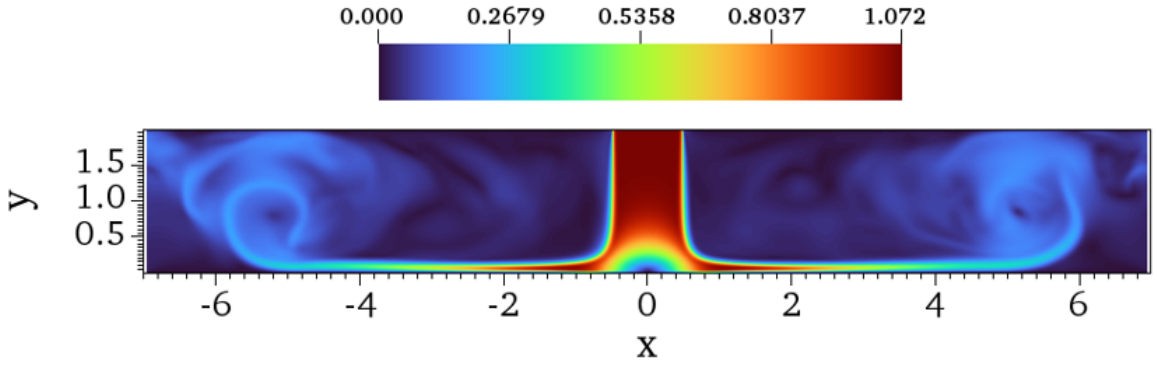

(a) Velocity magnitude

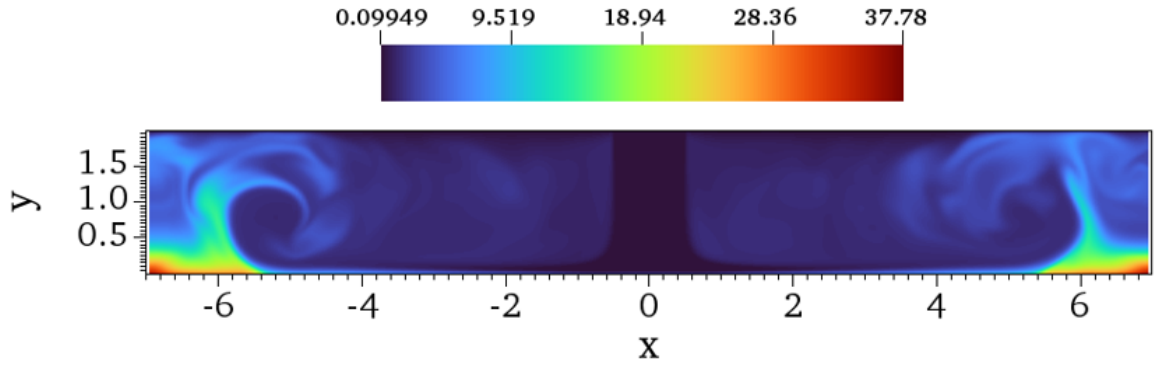

(b) Temperature

Figure 7: Velocity magnitude and temperature instantaneous sections ($z = 0$, $t = 125$).

instants (one coinciding with the local minimum of Nu_{stag}) have been identified, at which the behavior of the solution is studied.

In Fig. 6 the temperature and vorticity fields relative to the five time instants highlighted in Fig 5b are reported. The visualization clearly shows the cyclic generation of "new" vortices (NV) near the jet, which evolve to form the "primary" vortices (PV) impacting on the wall. Also, the formation of the "secondary" vortices (SV) near the wall is highlighted.

5. 3D simulations

In this section, a preliminary LES of a three-dimensional impinging jet is presented. Besides the difference due to the three-dimensional case itself, the configuration is the same one shown for the two-dimensional study. Thus, we are working with $Re = 2500$ and $Pr = 1$ on a computational grid sizes $\Omega = [-7,7] \times [0,2] \times [-7,7]$, with the boundary conditions presented in Sec. 3.

For the spatial discretization, a polynomial order $N = 8$ has been chosen and the initial grid is relatively coarser when compared to the two-dimensional case, counting $n_x \times n_y \times n_z \sim 150000$ hexahedral elements. The refinement near the wall is similar to what would have been used in a direct numerical simulation, due to the absence of a wall model, with $y^+ \approx 8$ for the first element of the grid. The filter used for the subgrid-scale model far from the wall affects the terms of the polynomial of order higher than five with a weight $\chi = 10$.

The simulation was performed until $t_f = 125$, and the time-averaged quantities have been calculated starting from $t_{\text{in}} = 50$. The time before the start of statistics collection is longer than in the two-dimensional case, since, due to the radial development of the fluid, more time is required to reach a developed configuration. To alleviate some numerical instabilities occurring in this case, the Courant number has been lowered to a target value of $c = 0.65$ and a second-

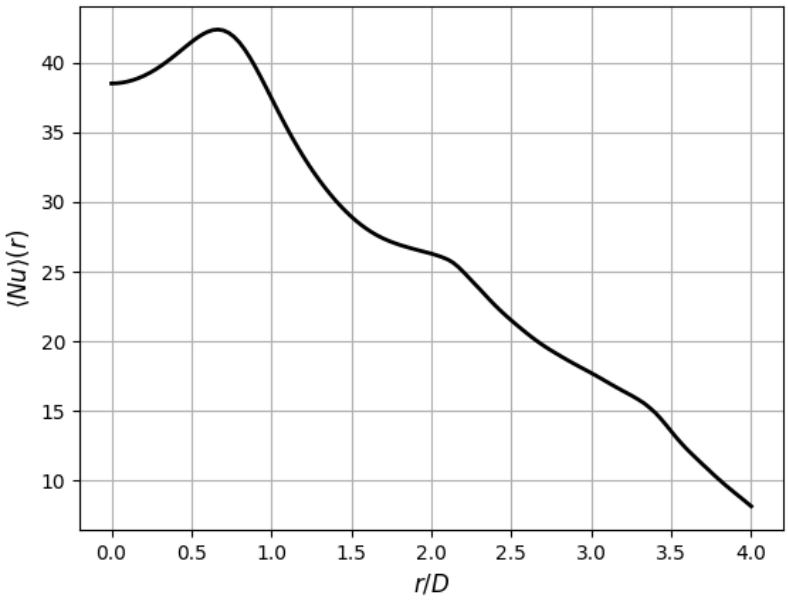

Figure 8: Time-averaged Nusselt number at the wall for the three-dimensional round impinging jet. Nusselt number calculated along the $x = z$ direction for positive x and z.

order method has been used.

Just as in the previous case, the three-dimensional simulation displayed no unnatural reflection due to the boundary condition and the vortices were able to exit the computational domain without causing the simulation to diverge. The instantaneous temperature and flow field at the end of the simulation are shown in Fig. 7 with a cross-section at $z = 0$. The results regarding the time-averaged Nusselt number at the wall are presented in Fig. 8. As observed from the experiments in [11], for low nozzle-to-plate values, the primary maximum for the average Nusselt number is not in correspondence of the jet axis, but it is further downstream. As shown in Fig. 8, the maximum happens at $r/D \approx 0.7$ which is similar to the value found by [7] at a higher Reynolds number of 10000. At $r/D \approx 2.1$ there is a change in the slope of the curve in correspondence of where the secondary maximum is expected. This is in line with what was reported in [5], in which it is shown that the LES models have not been able to capture the local minimum in between the primary and secondary maximum.

6. Conclusions

In this paper, the results of impinging jet simulations have been presented. The use of energy-stable boundary conditions have been tested to prevent the issues due to the presence of open boundaries. In both the two and three-dimensional cases, the simulations were free of non-physical reflections on the boundaries that would have otherwise affected the thermal and velocity field.

In the two-dimensional case, the vortical structures have been identified and studying the time-averaged Nusselt number at the wall the presence of a secondary maximum has been detected, apart from the primary one at the jet axis. In the three-dimensional case the primary maximum shifted at a radial distance $r/D \approx 0.7$ which is in line with what is reported in the literature for jet with low nozzle-to-plate distance. Due to the use of LES modelling, the secondary maximum is not clearly visible, but its presence can be detected through a slope change

in the Nusselt number curve.

The use of energy-stable boundary conditions has been shown to be able to attain physically correct results while using a smaller dominion then other methods, such as the fringe region technique, allowing for a reduction in computational cost. Future work would be to use this advantage to perform higher-fidelity simulation at higher Reynolds numbers.

Acknowledgment

Part of this work was supported by a grant of HPC time from CINECA under the ISCRA project CFDJets.

References

1. G.M. Carlomagno and A. Ianiro. Thermo-fluid-dynamics of submerged jets impinging at short nozzle-to-plate distance: A review. *Exp. Therm. Fluid Sci.*, 58:15–35, oct 2014.
2. J. Nordström, N. Nordin, and D. Henningson. The fringe region technique and the Fourier method used in the direct numerical simulation of spatially evolving viscous flows. *SIAM J. Sci. Comput.*, 20(4):1365–1393, jan 1999.
3. S. Dong and J. Shen. A pressure correction scheme for generalized form of energy-stable open boundary conditions for incompressible flows. *J. Comput. Phys.*, 291:254–278, 2015.
4. X. Liu, Z. Xie, and S. Dong. On a simple and effective thermal open boundary condition for convective heat transfer problems. *Int. J. Heat Mass Transf.*, 151:119355, apr 2020.
5. T. Dairay, V. Fortuné, E. Lamballais, and L.E. Brizzi. LES of a turbulent jet impinging on a heated wall using high-order numerical schemes. *Int. J. Heat Fluid Flow*, 50:177–187, dec 2014.
6. T.S. O'Donovan and D.B. Murray. Jet impingement heat transfer – Part I: Mean and root-mean-square heat transfer and velocity distributions. *Int. J. Heat Mass Transf.*, 50(17):3291–3301, 2007.
7. T. Dairay, V. Fortuné, E. Lamballais, and L.-E. Brizzi. Direct numerical simulation of a turbulent jet impinging on a heated wall. *J. Fluid Mech.*, 764:362–394, jan 2015.
8. S. Stolz, P. Schlatter, and L. Kleiser. High-pass filtered eddy-viscosity models for large-eddy simulations of transitional and turbulent flow. *Phys. Fluids*, 17(6):065103, 05 2005.
9. S. Patel, S, P.F. Fischer, M. Min, and A.G Tomboulides. An operator-integration-factor splitting (OIFS) method for incompressible flows in moving domains. Technical Report ANL/ALCF-17/8 140626, Argonne National Lab., 10 2017.
10. Y.M. Chung and K.H. Luo. Unsteady Heat Transfer Analysis of an Impinging Jet . *J. Heat Transfer*, 124(6):1039–1048, 12 2002.
11. J. Lee and S.-J. Lee. Stagnation region heat transfer of a turbulent axisymmetric jet impingement. *Exp. Heat Transf.*, 12(2):137–156, 1999.